

Article

# The Effects of the Properties of Gases on the Design of Bubble Columns Equipped with a Fine Pore Sparger

Athanasios G. Kanaris <sup>1</sup> , Theodosios I. Pavlidis <sup>2</sup>, Ariadni P. Chatzidafni <sup>2</sup>  
and Aikaterini A. Mouza <sup>2,\*</sup> 

<sup>1</sup> Scientific Computing Department, STFC, Rutherford Appleton Laboratory, Didcot OX11 0QX, UK; agkanaris@gmail.com

<sup>2</sup> Department of Chemical Engineering, Aristotle University of Thessaloniki, 54124 Thessaloniki, Greece; theodospi@auth.gr (T.I.P.); ariadni.chatzidafni@gmail.com (A.P.C.)

\* Correspondence: mouza@auth.gr; Tel.: +30-2310-994161

Received: 2 February 2018; Accepted: 7 March 2018; Published: 12 March 2018

**Abstract:** This work concerns the performance of bubble columns equipped with porous sparger and investigates the effect of gas phase properties by conducting experiments with various gases (i.e., air, CO<sub>2</sub>, He) that cover a wide range of physical property values. The purpose is to investigate the validity of the design equations, which were proposed in our previous work and can predict with reasonable accuracy the transition point from homogeneous to heterogeneous regime as well as the gas holdup and the mean Sauter diameter at the homogeneous regime. Although, the correlations were checked with data obtained using different geometrical configurations and several Newtonian and non-Newtonian liquids, as well as the addition of surfactants, the gas phase was always atmospheric air. The new experiments revealed that only the use of low-density gas (He) has a measurable effect on bubble column performance. More precisely, when the low-density gas (He) is employed, the transition point shifts to higher gas flow rates and the gas holdup decreases, a fact attributed to the lower momentum force exerted by the gas. In view of the new data, the proposed correlations have been slightly modified to include the effect of gas phase properties and it is found that they can predict the aforementioned quantities with an accuracy of  $\pm 15\%$ . It has been also proved that computational fluid dynamics (CFD) simulations are an accurate means for assessing the flow characteristics inside a bubble column.

**Keywords:** bubble column; porous sparger; holdup; bubble size; transition point; computational fluid dynamics

## 1. Introduction

Bubble columns are gas-liquid contactors that offer many advantages, because their construction is simple, their operating cost is low, and they can offer high-energy efficiency and good mass transfer capabilities. Consequently, they are widely used in many industrial gas-liquid operations (e.g., gas/liquid reactions, agitation by gas injection, fermentations, waste water treatment, etc.) in chemical and biochemical industries [1,2]. In all these processes, gas holdup and bubble size distribution are important design parameters, since they can be used to define the gas-liquid interfacial area available for mass transfer. In turn, these parameters depend strongly on the operating conditions, the physicochemical properties of the two phases, the gas sparger type and the column geometry [3,4]. Depending on the gas flow rate, two main flow regimes are generally encountered in bubble columns, namely the homogeneous bubbly flow regime, which corresponds to relatively low gas velocities and the heterogeneous (churn-turbulent flow) regime, which corresponds to higher gas

velocities. The homogeneous regime is characterized by discrete bubbles and can be classified into mono-dispersed homogeneous flow regime and in pseudo-homogeneous flow regime. The term pseudo-homogeneous is used to describe the flow regime in which the bubbles generated from the sparger are discrete but not uniform. In the heterogeneous regime the bubble interactions are more pronounced resulting to the formation of larger bubbles, which ascend with higher velocity. In the homogeneous regime the interfacial contact area per unit mass of air is larger and thus it is most desirable for practical applications [5], especially those involving sensitive materials (e.g., bioreactors, blood oxygenators) [6,7], since it also provides a low shear rate environment. The mechanism of bubble formation is of crucial importance to bubble column hydrodynamics. Figure 1 and Table 1 show the forces that act on an under-formation bubble (Equations in Table 1). A bubble is detached, when the sum of the upward forces (i.e., buoyancy, gas momentum, pressure) outweighs the sum of the downward ones (i.e., drag, inertial, surface tension).

In previous works conducted in this laboratory [4,8–10] we have experimentally studied the effect of the sparger characteristics (i.e., diameter, pore size), the liquid physical properties and the gas flow rate on the performance of a bubble column equipped with a fine pore sparger. We have employed both Newtonian and non-Newtonian liquids as well as liquids containing surfactants. Using the experimental data and based on dimensional analysis, we have formulated correlations that are based on dimensionless groups and can predict with reasonable uncertainty (better than  $\pm 15\%$ ) the transition point between the homogeneous and the heterogeneous regime as well as the gas holdup and the bubble size distribution at the homogeneous regime. However, these correlations use data where the gas phase is air, although several bubble column applications use other gases (e.g.,  $\text{CO}_2$ ) and in this case the different gas density affects the amplitude of the forces that act on an under-formation bubble.

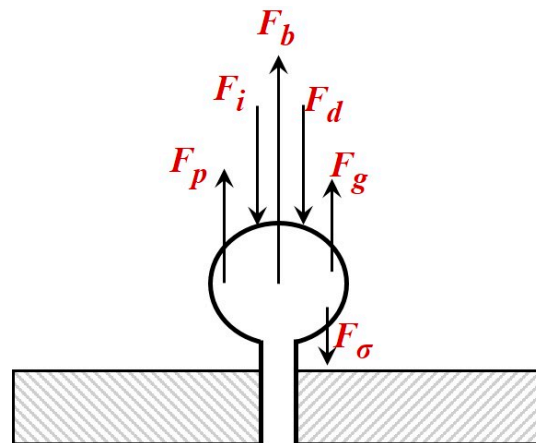


**Figure 1.** Forces acting on an under-formation bubble (Table 1).

**Table 1.** Forces acting during bubble formation.

Upward Forces	Downward Forces
Buoyancy: $F_b = (\rho_L - \rho_G)gV_b$	Drag: $F_d = \frac{1}{2}\rho_L W^2 \frac{\pi d_p^2}{4} C_D$
Gas momentum: $F_G = \frac{\pi}{4} d_p^2 \rho_G W_G^2$	Inertial: $F_i = \left( a_i + \frac{\rho_G}{\rho_L} \right) \rho_L V_b \gamma_b$
Pressure: $F_p = \frac{\pi}{4} d_p^2 (P_G - P_L)$	Surface tension: $F_\sigma = \pi d_p \sigma$

Thus, the purpose of this work is to check the validity of previously proposed correlations, by conducting experiments with several gases and, if necessary, to modify them to incorporate the effect of gas type. We will also use the experimental data to investigate the ability of a commercial CFD code to accurately simulate the performance of a bubble column and consequently to predict the flow characteristics (e.g., velocity profile, hold up distribution etc.) inside the column.

## 2. Experimental Set-Up and Procedure

The experimental set-up (Figure 2) consists of a cylindrical bubble column, equipped with a fine pore sparger for the injection and the uniform distribution of the gas phase, an appropriate flowmeter for gas flow control, a high speed digital video camera (Redlake MotioScope PCI<sup>®</sup> 1000S, DEL Imaging, Cheshire, CT, USA) for bubble size and gas holdup measurements and a computer for acquiring and processing the data. A Plexiglas<sup>®</sup> rectangular box, filled with the same fluid as the one used at the corresponding experiment was placed around the bubble column to eliminate image distortion caused by light refraction.

The gas phase is introduced the column through a fine pore sparger, namely a 316 L SS porous disk (Mott Corp.<sup>®</sup>, Farmington, CT, USA) with a nominal pore size of 40  $\mu\text{m}$  or 100  $\mu\text{m}$ , that covers the whole bottom plate. The effect of the sparger to column diameter ratio on the bubble column performance has been investigated and discussed in a previous paper [9]. To ensure that the gas phase is evenly distributed over the whole sparger area, the gas phase was injected through a 1 cm nozzle to a vessel of 35 cm height placed beneath the bubble column, following the design proposed in a previous paper [9]. A recording rate of 125 frames per second (fps) was used for the measurement of gas holdup, while a speed of 500 fps was selected for measuring the bubble size.

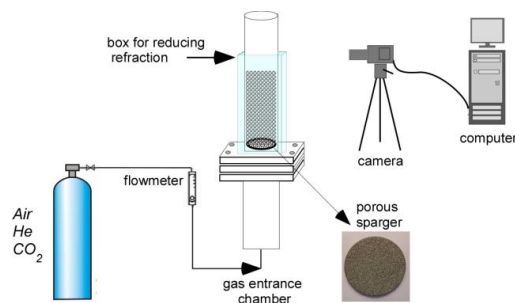


Figure 2. Experimental set-up.

The geometrical characteristics of the bubble columns studied are given in Table 2. The liquid phase was either de-ionized water or an aqueous glycerin solution (Table 3), while three gases, namely air, CO<sub>2</sub> and He, covering a sufficiently wide range of density values (Table 4) were individually employed. All the experiments were performed with no liquid throughput, at atmospheric pressure and ambient temperature conditions (i.e., around 20 °C).

Table 2. Bubble column characteristics.

$d_c$ (cm)	$d_s$ (cm)	$d_p$ ( $\mu\text{m}$ )	$d_p$ min ( $\mu\text{m}$ )	$d_p$ max ( $\mu\text{m}$ )
5	5	100	5	500
9	9	40	3	70

Table 3. Liquid phase properties.

Liquid	$\rho_L$ (Kg/m <sup>3</sup> )	$\mu_L$ (mPa·s)	$\sigma_L$ (mN/m)
water	1000	1.0	72
aqueous glycerin 40% $v/v$	1117	5.8	64

Table 4. Gas phase properties.

Gas	$\rho_G$ (Kg/m <sup>3</sup> )	$\mu_G$ (10 <sup>-5</sup> Pa·s)
Air	1.39	1.8
CO <sub>2</sub>	2.11	1.5
He	0.19	2.0

The average gas holdup ( $\varepsilon_G$ ) is estimated by calculating the bed expansion as follows:

$$\varepsilon_G = \frac{\sum_{i=1}^n \varepsilon_{G,i}}{n} = \frac{\sum_{i=1}^n \frac{H_i - H_{o,i}}{H_i}}{n} = \frac{\sum_{i=1}^n \frac{\Delta H_i}{H_i}}{n} \quad (1)$$

where  $H_0$  and  $H$  is the liquid level before and after gas injection respectively,  $\Delta H$  is the liquid level difference and  $n$  is the number of recurrent measurements for each gas flow rate (in this case  $n = 50$ ). In all our experiments the estimated maximum uncertainty of the measurements is less than 15%.

From bubble images taken by the video camera the diameter of a sample of 100 bubbles was measured and the Sauter mean diameter ( $d_{32}$ ), was calculated:

$$d_{32} = \frac{\sum_i^N n_i d_{bi}^3}{\sum_i^N n_i d_{bi}^2} \quad (2)$$

where  $d_{bi}$  and  $n_i$  are the diameter and the number of the bubbles of size class  $i$  respectively and  $N$  is the number of classes used for the distribution. The minimum number of classes required for the construction of the size distributions,  $k$  was estimated by the Sturges' rule:

$$k = 1 + \log_2 S \quad (3)$$

where  $S$  is the sample size ( $\sim 100$  bubbles). The number of classes used for the construction of the distributions in the present work is 10 equal intervals. Aiming to avoid possible random errors that may be involved in the measuring procedure, we were repeating the same experiment 5 times and we were calculating  $d_{32}$  for each experiment.

### 3. Results and Discussion

#### 3.1. Bubble Size Distribution

Figure 3 illustrates typical bubble size distributions with the 40  $\mu\text{m}$  sparger ( $d_c = 9 \text{ cm}$ ), for all gases studied and for a constant  $U_{GS}$  value. As expected [4], the distributions are log-normal while regardless of the liquid phase only the low density He gas exhibits an observable effect on the bubble distribution curve. This can be attributed to the considerably lower momentum force exerted by the low density He gas (Table 1). However, the value of mean Sauter diameter is not considerably affected by the type of gas but is mainly affected by the type of liquid phase employed (Table 5).

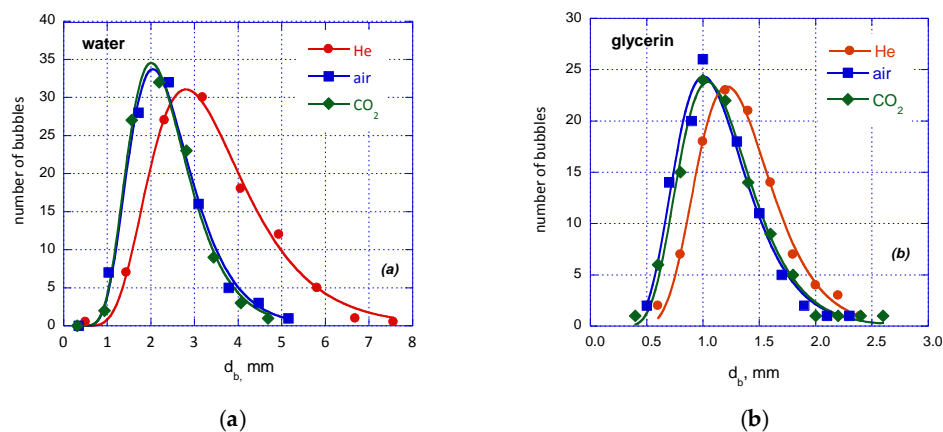


**Figure 3.** Effect of type of gas on bubble size distribution ( $U_{GS} = 0.01 \text{ m/s}$ ): (a) water; (b) glycerin sol.

**Table 5.** Measured mean Sauter diameter ( $U_{GS} = 0.01$  m/s,  $d_p = 40$   $\mu$ m).

Liquid	Gas	$d_{32}$ (mm)
water	Air	1.42
	He	1.50
	CO <sub>2</sub>	1.40
aqueous glycerin solution 40% v/v	Air	1.16
	He	1.24
	CO <sub>2</sub>	1.19

In previous works in our lab [4,9], a correlation for predicting the Sauter mean diameter ( $d_{32}$ ) based on dimensionless numbers was proposed. The same correlation can be used for predicting the mean Sauter diameter when different gases are employed provided that the constants of the correlation are suitably adjusted (Equation (4)).

$$\frac{d_{32}}{d_s} = 0.9 \left[ We^{0.95} Re_L^{0.40} Fr^{0.47} \left( \frac{d_p}{d_s} \right)^{0.55} \right]^{0.51} \quad (4)$$

where  $We$ ,  $Re$  and  $Fr$  are the Weber, Reynolds and Froude number respectively, based on gas superficial velocity and liquid phase properties and defined as:

$$We = \frac{\rho_L U_{GS}^2 d_c}{\sigma_L} \quad (5)$$

$$Re_L = \frac{U_{GS} d_c \rho_L}{\mu_L} \quad (6)$$

$$Fr = \frac{U_{GS}^2}{d_c g} \quad (7)$$

In Figure 4 it is shown that the proposed correlation (Equation (4)) can be used for predicting  $d_{32}$  values with reasonable accuracy (i.e.,  $\pm 15\%$ ) for all the gases employed.

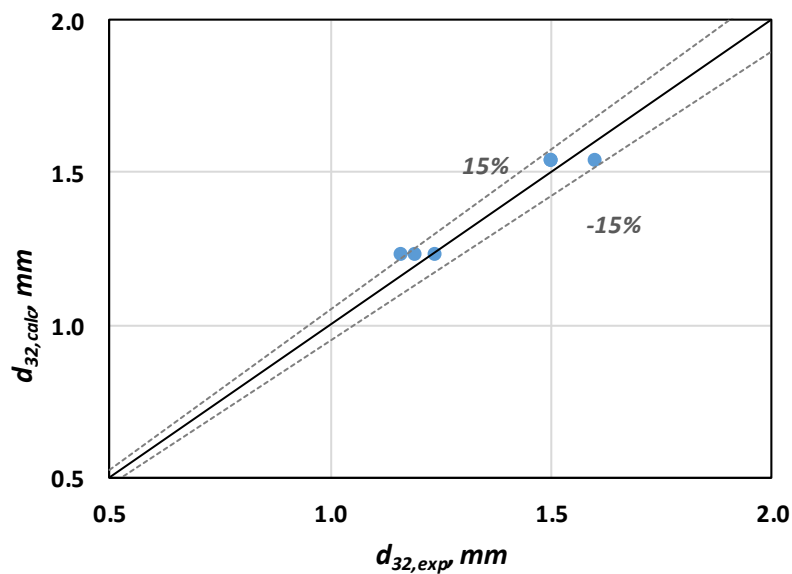


**Figure 4.** Comparison of the Sauter mean diameter prediction with experimental data (Table 5) ( $U_{GS} = 0.01$  m/s,  $d_p = 40$   $\mu$ m,  $d_c = 9$  cm).

### 3.2. Regime Transition

The transition point from homogeneous to heterogeneous regime is estimated by applying the drift flux analysis, which considers the relative motion of the two phases [11]. The basic quantity is the drift flux,  $j$ , is given by:

$$j = U_{GS}(1 - \varepsilon_G) \quad (8)$$

where  $\varepsilon_G$  is the gas holdup and  $U_{GS}$  is the superficial gas velocity defined as:

$$U_{GS} = \frac{Q_G}{A} \quad (9)$$

where  $Q_G$  is the gas flow rate and  $A$  the column cross section. When the drift flux is plotted versus the gas holdup, the change in the slope of the curve indicates the transition from homogeneous to heterogeneous regime [12].

The effect of the type of gas on regime transition is illustrated in Figure 5. It is obvious that, only when the lower density gas, He, is employed, the homogeneous regime is extended to higher  $j$  or equally  $U_{GS}$  values.

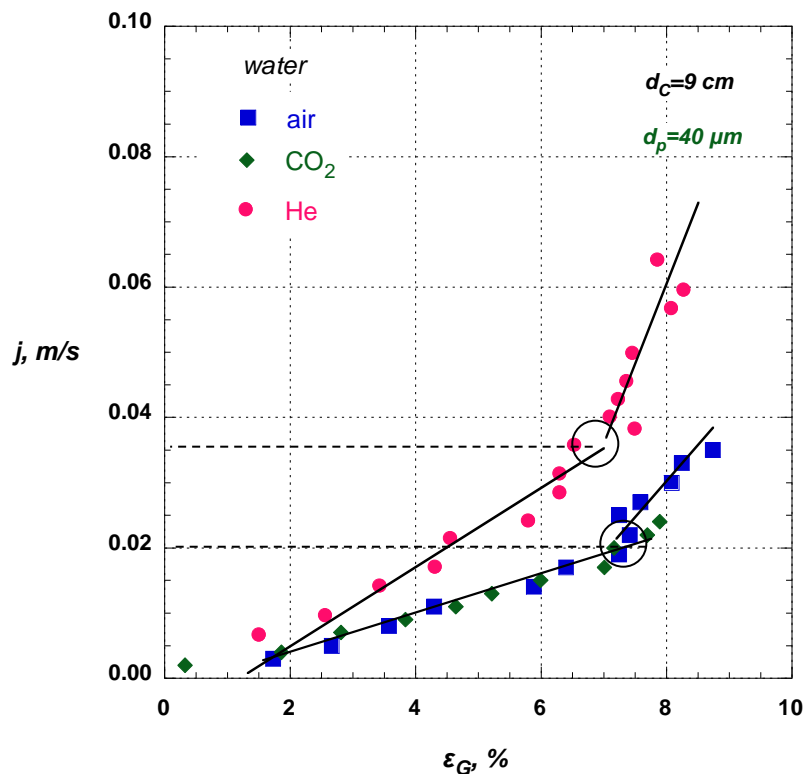


Figure 5. Effect of type of gas on regime transition for water ( $d_p = 40 \mu\text{m}$ ,  $d_c = 9 \text{ cm}$ ).

In previous papers [9,13], we have proposed a correlation (Equation (10)) for predicting the transition point that is based on dimensionless numbers and incorporates the physical properties of the liquid phase as well as the geometrical characteristics of the column and the porous sparger. This correlation has the general form:

$$Fr_{trans} = a_1 \left[ Eo^{a_2} \left( \frac{d_s}{d_c} \right)^{a_3} \right]^{a_4} \quad (10)$$

where  $Fr_{trans}$  is the Froude number at the transition point and  $Eo$  the Eotvos number based on  $d_{32}$ :

$$Fr_{trans} = \frac{U_{GS,trans}^2}{d_p g} \quad (11)$$

$$Eo = \frac{d_{32}^2 \rho_L g}{\sigma_L} \quad (12)$$

In view of the new results to incorporate the effect of type of gas, the ratio of gas density to that of air density is added. The new correlation is as follows:

$$Fr_{trans} = 1.2 \left[ Eo^{0.001} \left( \frac{d_s}{d_c} \right)^{0.02} \left( \frac{\rho_G}{\rho_{air}} \right)^{0.5} \right]^{0.005} \quad (13)$$

The predicted  $U_{GS,trans}$  values are in very good agreement, i.e., better than 15%, with the corresponding experimental data. The proposed correlation is suitable for predicting the transition point from homogeneous to heterogeneous regime.

### 3.3. Gas Holdup

In this section the effect of the various parameter on the gas holdup values is investigated. As it is expected, gas holdup increases with the gas velocity. The first part of the curve corresponds to the homogeneous regime, which is followed by a transition regime where the gas holdup slightly decreases. Finally, at the heterogeneous regime the gas holdup continues to increase, but with a lower slope than the homogeneous regime [8].

Figure 6 shows the dependence of gas holdup on corresponding gas superficial velocity for the two bubble columns used. It is obvious from that by increasing the column diameter the gas holdup increases, especially for higher gas flow rates. However, the literature results concerning the effect of column diameter on gas holdup are contradictory. Some researchers report that the column diameter has no effect on gas holdup [14–17]. The above works concern bubble columns with diameter larger than 10 cm, where the gas distributor is a perforated plate.

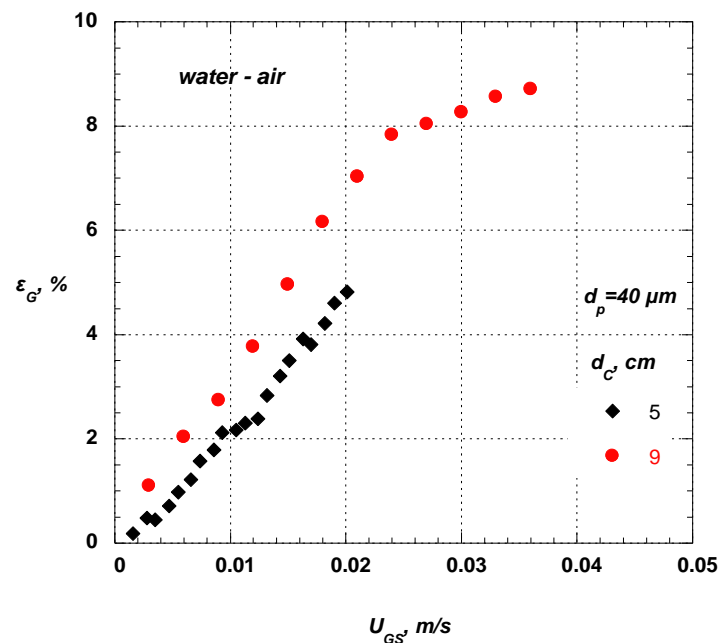


Figure 6. Effect of column diameter on gas holdup for the water-air system ( $d_p = 40 \mu\text{m}$ ).

Ruzicka et al. [18] also state that the gas holdup is independent of column dimensions provided that the column diameter is larger than 10 cm, the column height is larger than 15 cm and the column height to diameter ratio is more than 5. On the other hand, some works report that the column diameter affects the gas holdup. Botton et al. [19] report that gas holdup increases when the column diameter decreases, whereas Kumar et al. [20] who conducted experiments in bubble columns with diameters larger than 10 cm, state that there is a continuous increase in the gas holdup with increasing column diameter. To the best of our knowledge, there are no experimental results concerning bubble columns with diameter less than 10 cm, equipped with fine porous sparger. Dhotre et al. [21], who have numerically studied the effect of sparger type and height to diameter ratio on radial gas holdup profiles, report that for multipoint spargers, an increase of the column height to column diameter ratio results into marginal decrease of gas holdup. Obviously, when the column diameter decreases the wall effects become more intense.

Figure 7 presents typical effect of the type of gas on gas holdup. With increasing gas density gas holdup increases, e.g., helium that has a lower density exhibits lower values of gas holdup than air and CO<sub>2</sub>. This behavior is attributed to the fact that, the lower density gas exerts a lower momentum force to an under-formation bubble (Table 1). This observation agrees with other researchers [22,23] who also reported that gases of higher density produce higher gas holdup values, attributing this behavior on phenomena occurring during bubbles formation on the sparger. However, it is worth noticing that, even though the density of CO<sub>2</sub> is 50% higher than that of atmospheric air, for the lower gas superficial velocities both air and CO<sub>2</sub> exhibit almost the same behavior and only when the density decreases by more than 80% (i.e., for He) a noticeable change is observed (Figure 7).

In previous studies conducted in our lab [8,9,13] a correlation for predicting the average gas holdup,  $\varepsilon_G$ , was proposed based on dimensionless numbers. The equation has the general form:

$$\varepsilon_G = c_1 \left[ Fr^{c_2} Ar^{c_3} Eo^{c_4} \left( \frac{d_s}{d_c} \right)^{c_5} \left( \frac{d_p}{d_s} \right)^{c_6} \right]^{c_7} \quad (14)$$

where  $Fr$ ,  $Ar$  and  $Eo$  are the dimensionless Froude, Archimedes and Eotvos number respectively defined by:

$$Fr = \frac{U_{GS}^2}{d_c g} \quad (15)$$

$$Ar = \frac{d_c^3 \rho_L^2 g}{\mu_L^2} \quad (16)$$

$$Eo = \frac{d_c^2 \rho_L g}{\sigma_L} \quad (17)$$

the quantities  $d_c$ ,  $d_s$ , are the column and the sparger diameter, while  $d_p$  is the mean pore size of the sparger material. The values of constants  $c_1$  to  $c_7$  depend on the of liquid phase. It was also proved [8–10,13] that the proposed correlations can predict hold up with reasonable accuracy, i.e., better than 15%.

However, in the  $\varepsilon_G$  prediction, the type of gas is not taken into account although the gas momentum affects bubble evolution (Table 1). From Figure 7, where the effect of gas type is presented, it is apparent that only the very low density gas He has a measurable effect on gas holdup value. In case that the gas phase is other than air, it is necessary to introduce a term that incorporates the properties of the gas phase.

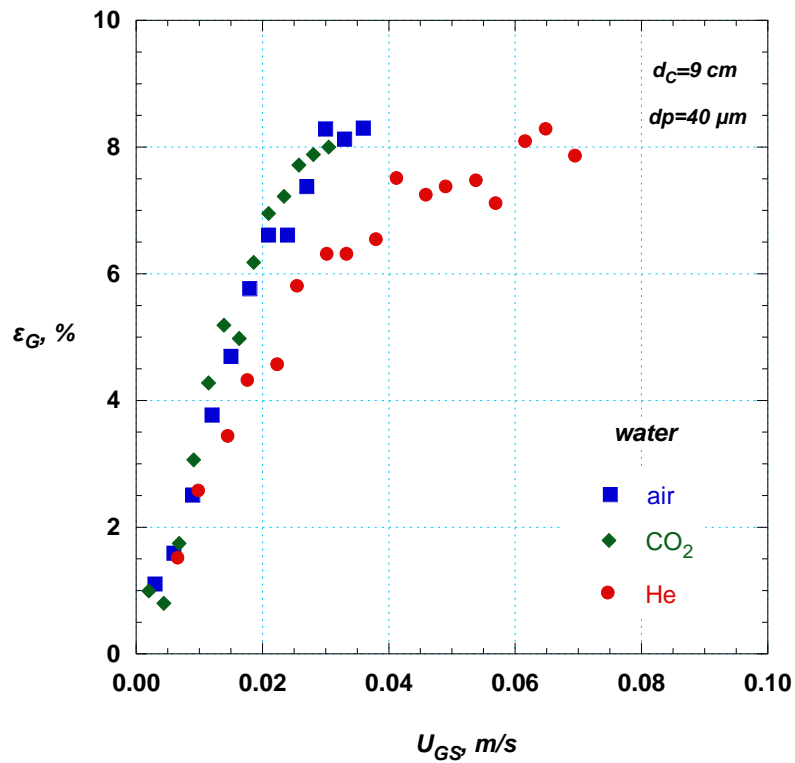


Figure 7. Effect of type of gas on gas holdup ( $d_p = 40 \mu\text{m}$ ,  $d_c = 9 \text{ cm}$ ).

Based on the above, we have modified Equation (10) by introducing in the gas Reynolds number  $Re_G$  defined as:

$$Re_G = \frac{U_{GS} d_c \rho_G}{\mu_G} \quad (18)$$

The modified form of the proposed correlation is as follows:

$$\varepsilon_G = c_1 \left[ Fr^{c_2} Ar^{c_3} Eo^{c_4} Re_G^{c_5} \left( \frac{d_s}{d_c} \right)^{c_6} \left( \frac{d_p}{d_s} \right)^{c_7} \right]^{c_8} \quad (19)$$

where the constants of the correlation are given in Table 6.

Table 6. Constants value for  $\varepsilon_G$  prediction equation (Equation (19)).

$C_1$	$C_2$	$C_3$	$C_4$	$C_5$	$C_6$	$C_7$	$C_8$
0.020	0.300	0.015	3.50	0.043	1.10	2.62	1.18

Figure 8 shows that the  $\varepsilon_G$  values predicted by Equation (19) are in very good agreement ( $\pm 15\%$ ) with the corresponding experimental data.

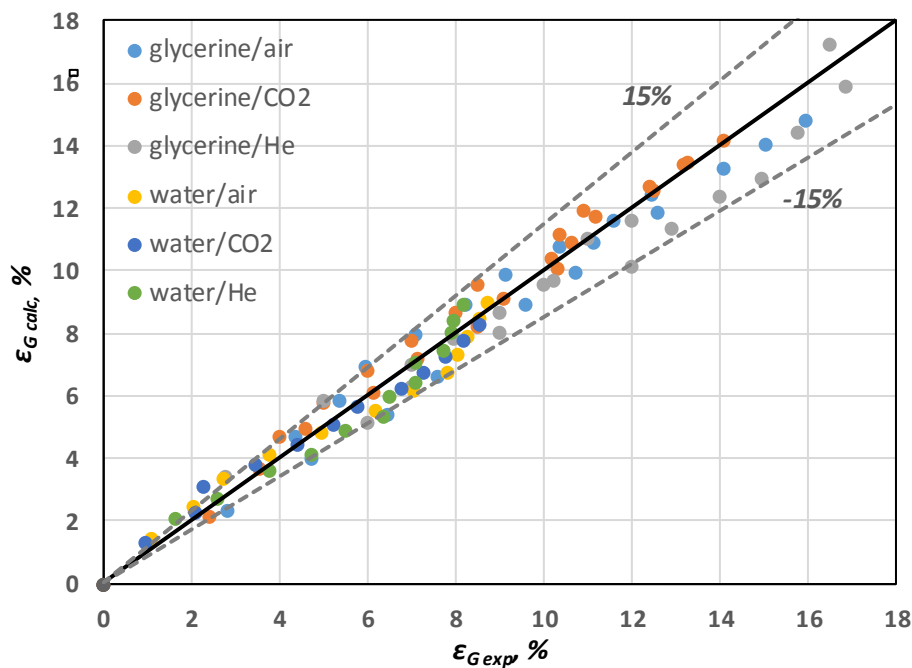


Figure 8. Comparison of the proposed correlation with the experimental data.

#### 4. Numerical Simulations

A method to gain more knowledge and detailed physical understanding of the hydrodynamics in bubble columns is the use of computational fluid dynamics (CFD). CFD can be regarded as an effective tool to clarify the importance of physical effects (e.g., gravity, surface tension) on flow by adding or removing them at will. An increasing number of papers deal with CFD application to bubble columns [3,9]. Vial et al. [24] cite the most important reasons for this interest. In this paper our intention is to validate the CFD code by comparing the numerical results with relevant experimental data. Then using the validate code we will be able to visualize the flow field inside the column.

The commercial CFD code ANSYS CFX 18.1, which was employed for the simulations, incorporates the MUSIG (Multiple Size Group) model to handle polydisperse multiphase flows, i.e., flows where the dispersed phase has wide size variation. In this case, the different sizes of the bubbles interact with each other through mechanisms of breakup and coalescence [25]. MUSIG starts by using the population balance equation to estimate the birth and death rates of bubbles due to breakup and coalescence. It requires the equation to use discretized size groups, whose initial conditions are provided by the user. In those size groups, the equal diameter discretization assumption is considered: the diameter represented by the group boundary is assumed to be midway between the diameters represented by the adjacent groups [25]. The mass represented by the upper limit of the largest-size group is based on the diameter represented by that limit, and the mass represented by the lower limit of the smallest-size group is assumed to be zero. MUSIG combines the population balance method with the break-up [26] and coalescence [27] models, to predict the bubble size distribution of the dispersed phase. It also uses the Eulerian–Eulerian two-phase model, and for the type of flow encountered in a bubble column, it is recommended to use the  $k$ - $\epsilon$  turbulent model for the continuous phase, while the dispersed phase is simulated with the zero-equation model. More details on the computational methods used are given in previous work by the authors [28]. The MUSIG model has led to success in the prediction of industrial bubbly flows [29], but it comes with limitations. The homogeneous MUSIG model is restricted to one gaseous phase velocity field applied to all bubble size classes. Also, the validity of bubble size distribution models falls exclusively within the inertial subrange of turbulence [30]. Therefore, to develop more reliable models, a more detailed turbulence energy spectrum model needs to be employed. However, this falls outside the scope of this study,

since the work involves convectively dominated bubbly flows where the assumptions mentioned hold truth [29].

All simulations were performed in time-dependent, transient mode, for the same total time length, i.e., 20 s. Due to the high computational demand, a parallel computing system was used, utilizing 24 AMD Opteron cores with 64 GB RAM. To ensure the accuracy of the results, a grid-dependence and a timestep-dependence study were performed for the higher air velocity tested. Gas holdup values were calculated for different grid size meshes up to 800,000 nodes, and for timesteps as small as 800 ms. It was found that the results are not significantly influenced by the timestep variation, while for grid densities more than 700,000 nodes gas holdup value is practically the same, thus this grid density was used for the remaining simulations, and a timestep of 800 ms was also used.

The simulations were validated by comparing the calculated holdup values with the relevant experimental ones. Table 7, where representative CFD results are presented, shows that the numerical simulation can quite accurately predict the hold up, i.e., achieving a deviation of less than 5%.

**Table 7.** Comparison of typical simulation results with the experimental data.

Liquid Phase	Gas Phase	$U_{GS}$ , m/s	$\epsilon_{G\text{ exp}}$ %	$\epsilon_{G\text{ calc}}$ %	Deviation %
water	He	0.02	5.9	5.6	5.0
		0.03	6.6	6.4	2.6
water	air	0.02	6.5	6.2	4.5
		0.03	7.9	8.0	0.7
aqueous glycerin 40% v/v	He	0.02	8.4	8.0	5.0

In Figure 9, typical CFD results concerning the evolution of gas volume fraction inside the bubble column (i.e., the bed expansion) is presented. The calculated gas holdup values given in Table 6 were predicted by calculating the liquid bed expansion. Figure 10 also presents typical contour plots at a randomly selected time snapshot, offering an insight on the expected distribution of shear stress of the liquid phase and streamlines formation.

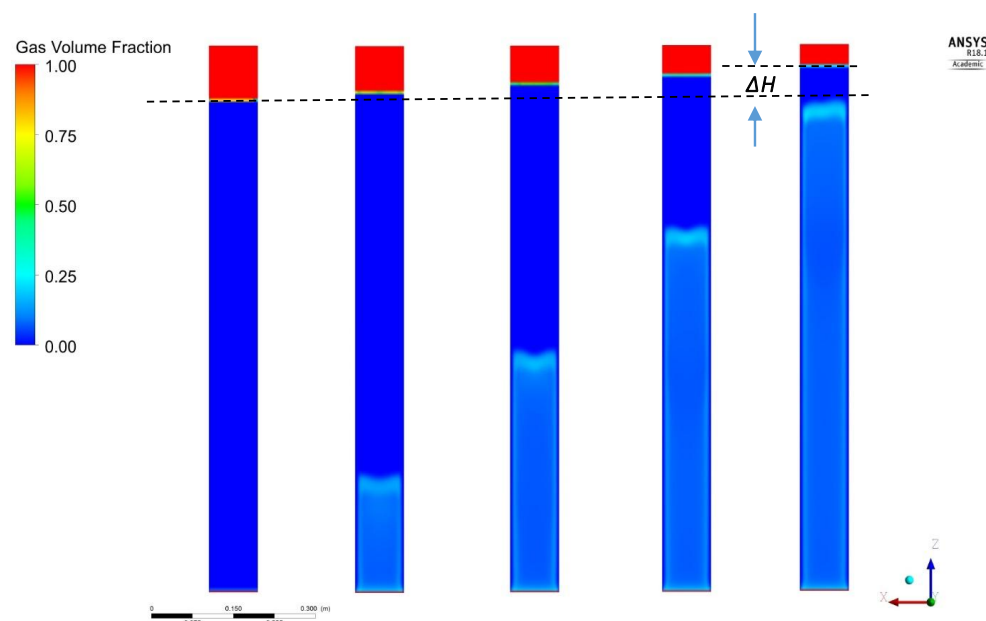


**Figure 9.** Bed expansion ( $\Delta H$ ) for different time snapshots:  $t = 0, 0.8, 1.6, 2.4$  and  $3.2$  s (air-water,  $U_{GS} = 0.2$  m/s,  $d_p = 40$   $\mu\text{m}$ ,  $d_c = 9$  cm).

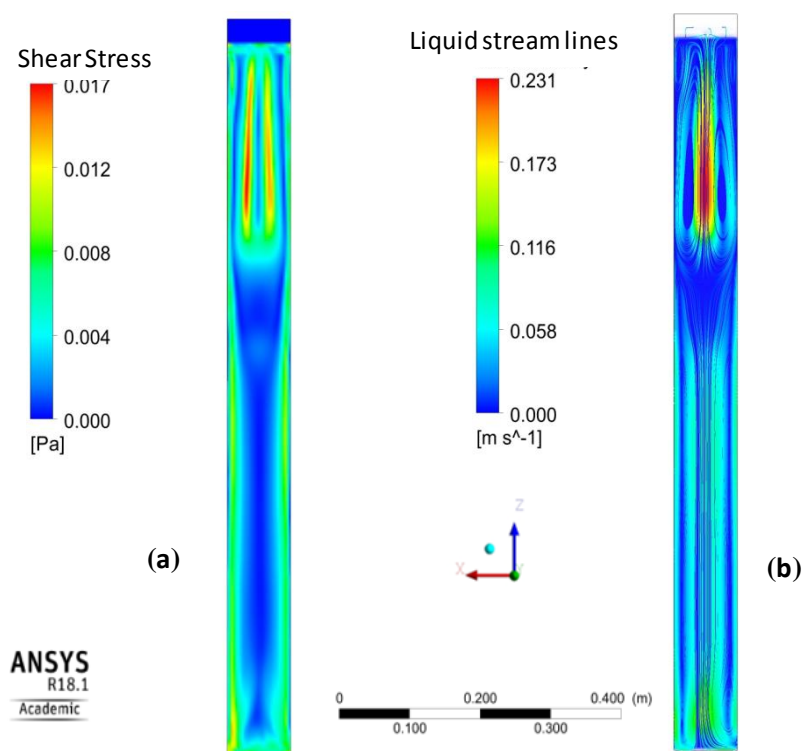


**Figure 10.** Typical CFD results at the middle plane of the bubble column: (a) Shear stress distribution; (b) Streamlines colored with the liquid phase velocity ( $t = 5.8$  s,  $U_{GS} = 0.2$  m/s, air-water,  $d_p = 40$   $\mu\text{m}$ ,  $d_c = 9$  cm).

## 5. Concluding Remarks

In this work, we have experimentally investigated in what extent the type of gas phase influences the performance of a bubble column reactor by employing gases that cover a wide range of physical properties, namely atmospheric air and  $\text{CO}_2$  exhibit almost the same behavior, while the low density He shows a measurable effect on bubble column design quantities. This can be attributed to the fact that the low density He gas exhibits a lower momentum force. Thus, the previously proposed correlations for predicting the transition point from the homogeneous to the heterogeneous regime, the gas holdup and the Sauter mean diameter are slightly modified to include the effect of the type of gas employed. The new correlations can predict the aforementioned quantities with reasonable accuracy (better than 15%). Relevant CFD simulations were also performed and validated with the available experiments results in terms of gas holdup. Thus, it has been demonstrated that CFD can be used for predicting the flow characteristics that are generally difficult to be experimentally measured, but are essential during bubble column design, as for example the shear stress or the velocity distribution.

**Acknowledgments:** The authors would like to thank Asterios Lekkas for the construction and installation of the experimental setup and Spiros V. Paras for his constructive comments.

**Author Contributions:** Aikaterini A. Mouza had the initial conception of this work and designed the experiments; Theodosios I. Pavlidis and Ariadni P. Chatzidafni conducted the experiments, acquired and analyzed the data; Athanasios G. Kanaris and Aikaterini A. Mouza performed the simulations; Aikaterini A. Mouza interpreted the results and wrote the manuscript. This work is not affiliated with the Science and Technology Facilities Council (STFC).

**Conflicts of Interest:** The authors declare no conflicts of interest.

## Nomenclature

$A$	column cross section, $m^2$
$d_b$	bubble diameter, m
$d_{32}$	Sauter mean diameter, m
$d_c$	column diameter, m
$d_p$	pore diameter, m
$d_s$	sparger diameter, m
$F_b$	buoyancy force, N
$F_d$	drag force, N
$F_g$	gas momentum force, N
$F_i$	inertial force, N
$F_p$	pressure force, N
$F_\sigma$	surface tension force, N
$g$	acceleration of gravity, $m/s^2$
$H_C$	column height, m
$j$	drift flux, m/s
$Q_G$	gas flow rate, $m^3/s$
$U_{GS}$	superficial gas velocity, m/s
$W_g$	bubble formation velocity, m/s
<i>Greek letters</i>	
$\varepsilon_G$	average gas holdup, dimensionless
$\mu_G$	gas phase viscosity Pa s
$\mu_L$	liquid phase viscosity, Pa s
$\rho_G$	gas density, $Kg/m^3$
$\rho_L$	liquid density, $Kg/m^3$
$\sigma_L$	surface tension, mN/m
<i>Dimensionless quantities</i>	
$Ar$	Archimedes number
$Eo$	Eotvos number
$Fr$	Froude number
$Fr_{tans}$	Froude number at transition point
$k$	minimum number of classes
$N$	number of classes used for the distributions
$n_i$	number of bubbles of size class $i$
$Re_L$	Reynolds number based on liquid properties
$Re_G$	Reynolds number based on gas properties
$S$	sample size
$We$	Weber number

## References

1. Deckwer, W.D. *Bubble Column Reactors*; Wiley: Chichester, UK, 1992.
2. Finch, J.A.; Dobby, G.S. *Column Flotation*; Pergamon Press: Oxford, UK, 1990.
3. Camarasa, E.; Vial, C. Influence of coalescence behaviour of the liquid and of gas sparging on hydrodynamics and bubble characteristics in a bubble column. *Chem. Eng. Process. Process Intensif.* **1999**, *38*, 329–344. [[CrossRef](#)]
4. Kazakis, N.A.; Mouza, A.A.; Paras, S.V. Experimental study of bubble formation at metal porous spargers: Effect of liquid properties and sparger characteristics on the initial bubble size distribution. *Chem. Eng. J.* **2008**, *137*, 265–281. [[CrossRef](#)]
5. Joshi, J.B.; Vitankar, V.S. Coherent flow structures in bubble column reactors. *Chem. Eng. Sci.* **2002**, *57*, 3157–3183. [[CrossRef](#)]

6. Dhanasekharan, K.M.; Sanyal, J. A generalized approach to model oxygen transfer in bioreactors using population balances and computational fluid dynamics. *Chem. Eng. Sci.* **2005**, *60*, 213–218. [[CrossRef](#)]
7. Jones, T.J.; Deal, D.D. How effective are cardiopulmonary bypass circuits at removing gaseous microemboli? *J. Extra Corpor. Technol.* **2002**, *34*, 34–39. [[PubMed](#)]
8. Mouza, A.A.; Dalakoglou, G.K.; Paras, S.V. Effect of liquid properties on the performance of bubble column reactors with fine pore spargers. *Chem. Eng. Sci.* **2005**, *60*, 1465–1475. [[CrossRef](#)]
9. Passos, A.D.; Voulgaropoulos, V.P.; Paras, S.V.; Mouza, A.A. The effect of surfactant addition on the performance of a bubble column containing a non-Newtonian liquid. *Chem. Eng. Res. Des.* **2015**, *95*, 93–104. [[CrossRef](#)]
10. Anastasiou, A.D.; Kazakis, N.A.; Mouza, A.A.; Paras, S.V. Effect of organic surfactant additives on gas holdup in the pseudo-homogeneous regime in bubble columns equipped with fine pore sparger. *Chem. Eng. Sci.* **2010**, *65*, 5872–5880. [[CrossRef](#)]
11. Isbin, H.S. One-dimensional two-phase flow, Graham B. Wallis, McGraw-Huill, New York (1969). *AIChE J.* **1970**, *16*, 896–1105. [[CrossRef](#)]
12. Shah, Y.T.; Kelkar, B.G. Design parameters estimations for bubble column reactors. *AIChE J.* **1982**, *28*, 353–379. [[CrossRef](#)]
13. Kazakis, N.A.; Papadopoulos, I.D.; Mouza, A.A. Bubble columns with fine pore sparger operating in the pseudo-homogeneous regime: Gas hold up prediction and a criterion for the transition to the heterogeneous regime. *Chem. Eng. Sci.* **2007**, *62*, 3092–3103. [[CrossRef](#)]
14. Yovel, Y.; Franz, M.O. Plant classification from bat-like echolocation signals. *PLoS Comput. Biol.* **2008**, *4*, e1000032. [[CrossRef](#)] [[PubMed](#)]
15. Forret, A.; Schweitzer, J.M. Influence of scale on the hydrodynamics of bubble column reactors: An experimental study in columns of 0.1, 0.4 and 1 m diameters. *Chem. Eng. Sci.* **2003**, *58*, 719–724. [[CrossRef](#)]
16. Wilkinson, P.M.; Spek, A.P.; van Dierendonck, L.L. Design parameters estimation for scale-up of high-pressure bubble columns. *AIChE J.* **1992**, *38*, 544–554. [[CrossRef](#)]
17. Vatai, G.Y.; Tekić, M.N. Gas hold-up and mass transfer in bubble columns with pseudoplastic liquids. *Chem. Eng. Sci.* **1989**, *44*, 2402–2407. [[CrossRef](#)]
18. Ruzicka, M.C.; Drahoš, J. Effect of bubble column dimensions on flow regime transition. *Chem. Eng. Sci.* **2001**, *56*, 6117–6124. [[CrossRef](#)]
19. Botton, R.; Cosserat, D.; Charpentier, J.C. Influence of column diameter and high gas throughputs on the operation of a bubble column. *Chem. Eng. J.* **1978**, *16*, 107–115. [[CrossRef](#)]
20. Kumar, S.B.; Moslemian, D.; Duduković, M.P. Gas-holdup measurements in bubble columns using computed tomography. *AIChE J.* **1997**, *43*, 1414–1425. [[CrossRef](#)]
21. Dhotre, M.T.; Ekambara, K.; Joshi, J.B. CFD simulation of sparger design and height to diameter ratio on gas hold-up profiles in bubble column reactors. *Exp. Therm. Fluid Sci.* **2004**, *28*, 407–421. [[CrossRef](#)]
22. Hecht, K.; Bey, O. Effect of Gas Density on Gas Holdup in Bubble Columns. *Chemie Ingenieur Technik* **2015**, *87*, 762–772. [[CrossRef](#)]
23. Krishna, R.; Wilkinson, P.M.; Van Dierendonck, L.L. A model for gas holdup in bubble columns incorporating the influence of gas density on flow regime transitions. *Chem. Eng. Sci.* **1991**, *46*, 2491–2496. [[CrossRef](#)]
24. Vial, C.; Lainé, R. Influence of gas distribution and regime transitions on liquid velocity and turbulence in a 3-D bubble column. *Chem. Eng. Sci.* **2001**, *56*, 1085–1093. [[CrossRef](#)]
25. ANSYS. *CFX-Solver Theory Guide*; ANSYS: Canonsburg, PA, USA, 2017.
26. Luo, H.; Svendsen, H.F. Theoretical model for drop and bubble breakup in turbulent dispersions. *AIChE J.* **1996**, *42*, 1225–1233. [[CrossRef](#)]
27. Prince, M.J.; Blanch, H.W. Bubble coalescence and break-up in air-sparged bubble columns. *AIChE J.* **1990**, *36*, 1485–1499. [[CrossRef](#)]
28. Mouza, A.A.; Kazakis, N.A.; Paras, S.V. Bubble column reactor design using a CFD code. In Proceedings of the 1st International Conference “From Scientific Computing to Computational Engineering”, Athens, Greece, 8–10 September 2004.

29. Frank, T.; Zwart, P.J.; Shi, J.-M.; Krepper, E.; Lucas, D.; Rohde, U. Inhomogeneous MUSIG Model—A Population Balance Approach for Polydispersed Bubbly Flows. In Proceedings of the International Conference Nuclear Energy for New Europe, Bled, Slovenia, 5–8 September 2005.
30. Solsvik, J.; Jakobsen, H.A. Development of fluid particle breakup and coalescence closure models for the complete energy spectrum of isotropic turbulence. *I&EC Res.* **2016**, *55*, 1449–1460. [[CrossRef](#)]



© 2018 by the authors. Licensee MDPI, Basel, Switzerland. This article is an open access article distributed under the terms and conditions of the Creative Commons Attribution (CC BY) license (<http://creativecommons.org/licenses/by/4.0/>).